Thin Solid Films 574 (2015) 162–168

Contents lists available at ScienceDirect

Thin Solid Films

journal homepage: www.elsevier.com/locate/tsf

Effect of thickness on structural and electrical properties of Al-doped ZnO films

F.A. Garcés [a,*], N. Budini [a], R.D. Arce [a,b], J.A. Schmidt [a,b]

[a] Instituto de Física del Litoral (CONICET-UNL), Güemes 3450, Santa Fe S3000GLN, Argentina
[b] Facultad de Ingeniería Química, Universidad Nacional del Litoral, Santiago del Estero 2829, Santa Fe S3000AOM, Argentina

ARTICLE INFO

Article history:
Received 27 June 2014
Received in revised form 4 December 2014
Accepted 5 December 2014
Available online 11 December 2014

Keywords:
Mosaicity
Sol–gel
Thin film
Zinc oxide
Electrical properties

ABSTRACT

In this work, we have investigated the influence of thickness on structural and electrical properties of Al-doped ZnO films. Transparent conducting oxide films were grown by the spray pyrolysis technique from precursors prepared via the sol–gel method. We determined the structural properties of the films by performing X-ray diffraction and mosaicity measurements, which evidenced an increase of disorder and inhomogeneity between crystalline domains as the films thickened. This behavior was contrasted with results obtained from electrical measurements and was attributed to plastic deformation of the films as their thickness increased. As a result, the carrier mobility, the optical gap and the activation energy are affected due to emerging grain boundaries and a higher degree of disorder.

1. Introduction

Intrinsic and doped ZnO thin films are currently under investigation and development for applications in optoelectronics and energy conversion. In particular, transparent and conductive Al-doped ZnO (AZO) films are being considered for manufacturing transparent electrodes in flat panel displays, solar cells and organic devices due to their high electro-optical quality, high material availability and low cost for large area applications [1–3]. Many techniques have arisen to deposit ZnO films on different substrates, such as sol–gel method [4], spray pyrolysis [5], metal-organic chemical vapor deposition [6], pulsed laser deposition [7], molecular beam epitaxy [8] and sputtering [9]. Among these, the spray pyrolysis method has gained increased interest during the last years due to some advantages in comparison to other methods. It is simple and easy to implement, produces high purity films and provides excellent control of chemical uniformity. This non-expensive method was initially developed for transparent conducting oxide deposition in solar cell applications since the process is flexible and allows simple modifications for large area depositions. Regarding the chemical spray technique, ZnO thin films are frequently deposited by pyrolytic reaction of zinc acetate dissolved in an alcoholic solution. To obtain films with high conductivity, F, In, Ga and Al are some of the most used dopants. In the case of Al, every ion of the dopant can replace a Zn atom in the structure and release a free electron, which increases the free carrier concentration [10,11]. Up to now, Al has been used as an effective dopant to increase the conductivity of ZnO films, allowing it to reach about 500 Ω^{-1} cm^{-1} while maintaining an average transmittance of 85% in the visible region of the spectrum [11]. In addition, a preferential growth in either the (0 0 2) or the (1 0 1) plane is obtained, depending on the deposition conditions.

In a recent work, we have studied the effect of thickness on the structural and electrical characteristics of SnO_2:F thin films, synthesized by the sol–gel method and deposited by spray pyrolysis [12]. We have found a strong relation between thickness and crystalline domain misorientation or mosaicity, which also influences the electronic transport. Consequently, in the present study we have used the same methodology (i.e. sol–gel and spray pyrolysis) to deposit and study transparent conducting AZO films with different thicknesses, varying only the deposition time. In this context, we investigated the effect of film thickening on the evolution of morphological, electrical and optical properties. The correlation between structural properties, mosaicity, optical, and electrical properties of these films is discussed.

2. Experimental details

We synthesized the AZO ethoxylated precursors from Zn salts [Sigma-Aldrich 99.999% $Zn(O_2CCH_3)_2(H_2O)_2$, 0.2 M] and Al dopant through the sol–gel method [13]. The Al source was, in this case, the $AlCl_3 \cdot 6H_2O$ compound (Sigma-Aldrich 99.0%). Subsequently, a spray pyrolysis process allowed us to deposit AZO thin films onto glass substrates (Borofloat®) [12]. To fabricate samples with different thicknesses, the deposition times were varied in the range from 5 to 30 min, namely 5, 15, 20, 25 and 30 min. These times led to thicknesses

* Corresponding author. Tel.: +54 342 4559175x2065/2183.
E-mail address: felipe.garces@santafe-conicet.gov.ar (F.A. Garcés).

http://dx.doi.org/10.1016/j.tsf.2014.12.013
0040-6090/

of 0.43, 0.67, 0.80, 1.26 and 1.40 μm, respectively. A triethylamine (Sigma-Aldrich >99% $C_6H_{15}N$) solution was used as an additive for the sol–gel process. The precursors were gauged in a total volume of 100 ml by using solvents like ethanol and water. Generally, the deposition temperature used for ZnO fabrication is in the range between 380 and 500 °C [14]. In this work we have used a temperature of 450 °C, which was chosen after optimizing the conductivity and transparency of the deposited films. The Al concentration was fixed taking into account the fraction Al/Zn and, in this case, was 1.0%. It is worth noting that this concentration corresponds to the precursor in solution.

To have an insight on the structural characteristics of the samples we performed X-ray diffraction (XRD) measurements in the typical θ–2θ Bragg–Brentano configuration. In this way, we looked for the presence of ZnO characteristic diffraction peaks to prove the existence of crystalline domains in the films. The patterns were normalized to account for thickness differences between samples. Structural mosaicity, or tilting between crystalline domains (see details in Ref. [12]), was also determined by XRD measurements. This was accomplished by rocking the incidence angle (θ) in 2° steps while scanning the diffracted intensity at the diffraction angle (2θ) around the maximum of the selected peak, centered at (θ_{hkl}, $2\theta_{hkl}$). Here, (hkl) are the Miller indices of the corresponding diffracting plane. This configuration and procedure have been reported by Marty et al. [15] and we have also described it in Ref. [12]. The diffraction patterns were subsequently integrated over the scanned 2θ range to obtain the rocking curves as a function of $\Delta\theta$ ($=\theta - \theta_{hkl}$), whose width measures directly the degree of mosaicity or overall tilting between crystalline domains. The XRD measurements were carried out in a SHIMADZU XD-D1 diffractometer, operating with the Cu K_α line ($\lambda = 1.541$ Å). Film thickness was determined by direct transmittance measurements, in a Shimadzu UV3600 spectrophotometer. Surface roughness and texture were inspected by atomic force microscopy (AFM) measurements, performed in a NANOTEC probe system.

In turn, the electrical characterization was achieved by measuring conductivity as a function of temperature, in a vacuum chamber with temperature control, and performing Hall effect measurements, at room temperature by the Van der Pauw method.

3. Results and discussion

AFM images are generally used to characterize the morphology of the surface, by means of root–mean–square (RMS) roughness, and to determine the grain size. Our layers presented a quite uniform surface morphology dominated by hexagonal structures, as shown in Fig. 1 for the different deposition times. The shape of the grains is shown augmented in the inset of each AFM image. At the lower right of Fig. 1 we plot the variation of RMS roughness as a function of the film thickness. Normally, RMS roughness gradually enlarges as thickness increases, which is the observed trend for our samples. As thickness reached its highest value (1.40 μm) RMS roughness grew monotonically to 65 nm. This behavior is consistent with the results obtained from XRD measurements, as will be shown later. The hexagonal morphology observed on the surface is attributable to oriented growth in the [0 0 2] direction of ZnO wurtzite phase [16]. RMS roughness increased for thicker samples due to the stacking of successive layers possessing these hexagonal structures oriented in different directions with respect to the substrate normal. We also observed that, besides the stacking of these hexagonal-shaped nanosheets, there was an enlargement of the hexagons that form these stacked structures. For a film thickness of around 0.6 μm (Fig. 1, 0.42 and 0.67 μm) the grains grew to about 0.2 μm. It is likely that the stacking of nanosheets, for thicknesses between 0.80 and 1.4 μm, gives place to a pyramidal structure as shown in Fig. 1 for longer deposition times.

As reported by Owen et al., the chemical termination of the surface affects the characteristics of the next layer during the growth process [17]. The authors proposed a flipping of grain polarity from O- to Zn-termination during growth. This would cause that faster progressing Zn-terminated growth overtakes neighboring O-terminated material, leading to textured growth. In our samples, the different sizes of features on the surface (Fig. 1) would be due to the *c* axis polarity flipping at different points during growth.

The changes in the shape of ZnO grains as a function of film thickness can be explained by the transformation of growth model. During the deposition of thinner films, the grains grow approximately following a 2D model [18]. This results in the formation of hexagonal-shaped ZnO nanosheets with a high width/thickness ratio of up to 10. However, as

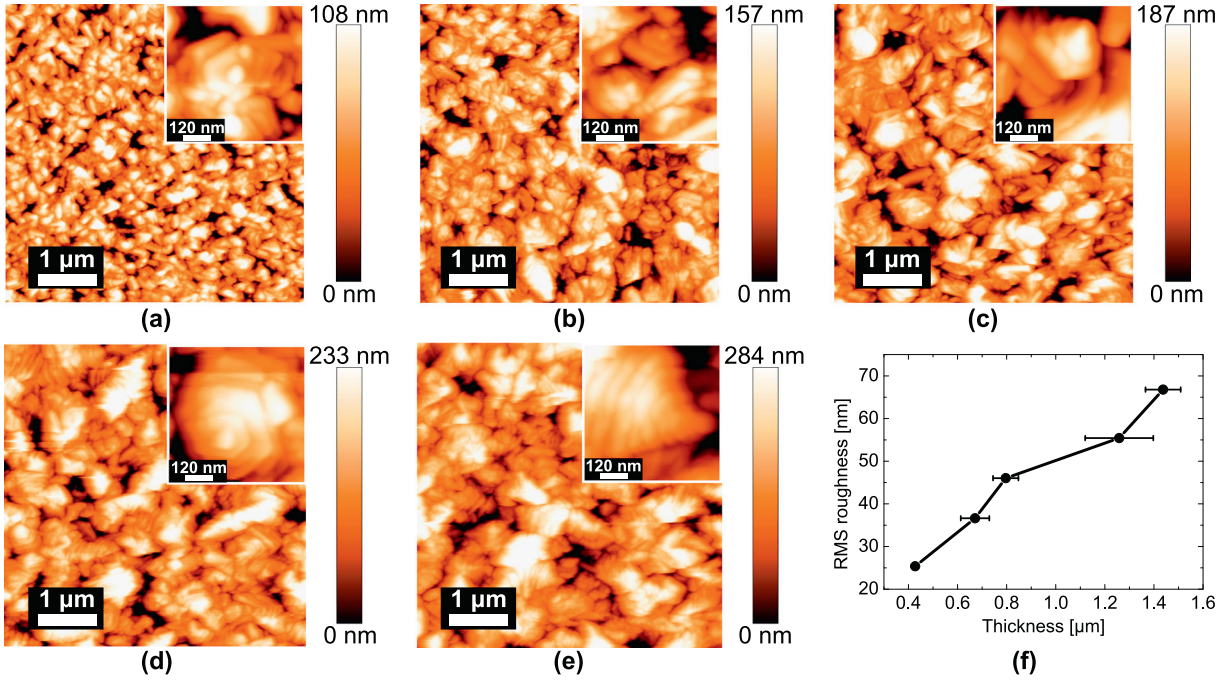

Fig. 1. Atomic force microscopy images for AZO films with different thicknesses, obtained by spray pyrolysis after a deposition time of (a) 5 min, (b) 15 min, (c) 20 min, (d) 25 min and (e) 30 min. Figure (f) shows the RMS roughness of the resulting films as a function of the thickness obtained for each deposition time.

thickness increases the grains tend to grow following a 3D model. Therefore, the grain shape changes to a pyramidal structure. In short, the grain size increases and the grain shape changes from hexagonal to pyramidal as the film gets thicker.

Fig. 2(a) shows the optical transmittance of AZO films with different thicknesses. The films resulted quite transparent in the visible region of the spectrum. The transmittance reached a maximum value of 90% for wavelengths near 650 nm for the 0.43 μm-thick sample. For thicker samples the transmittance resulted lower, which is attributed mainly to a higher scattering produced by the increasing film roughness. The diminution observed towards 380 nm is due to absorption at the semiconductor band gap and to Rayleigh scattering caused by surface roughness, which increases as λ^{-4} (provided the vertical RMS roughness of the scattering surface is much smaller than the wavelength of the incident light) [19]. However, there was a shift in the absorption band edge [see Fig. 2(b)], which can be explained by the increase of carrier concentration and blocking of low energy transitions [20,21]. To calculate the optical band gap energies of the films, we used the absorption coefficient $\alpha \propto -\ln(T/T_0)$ corresponding to the band gap of ZnO wurtzite structure. In Fig. 2(b), we plot $[\alpha(h\nu)]^2$ against the photon energy, $h\nu$. By extrapolating the linear region of these curves (at higher energies) we determined the optical gap value of the films as their intersections with the horizontal axis. The inset of Fig. 2(b) shows the obtained gap values as a function of film thickness.

Interestingly, the band gap energy of the AZO layers decreased slightly with thickness. In general, band gap energy variations in ZnO thin films are related to changes in mean crystallite size, internal stress and/or free carrier concentration [22–26]. It is well-known that two competing phenomena affect the band gap energy values as donor density increases, mainly in heavily doped semiconductors [27]. The first is related to a gap widening due to the band-filling effect, known as Burstein–Moss (B–M) effect [20]. This phenomenon involves a gap widening in highly *n*-doped materials as the carrier concentration increases, owing to a blocking of lowest states of conduction band by excess electrons [25]. The second phenomenon affects the gap of ZnO films for carrier concentrations above the Mott critical concentration ($\sim 5 \times 10^{18}$ cm^{-3}) because the electron–electron and electron–impurity interactions give rise to an energy shift of the valence and conduction bands, reducing the band gap [27]. This has been attributed to the merging of an impurity band into the conduction band, thereby shrinking the band gap. In many materials, this transition is observable as a disappearance of the conductivity activation energy. This particular feature was not observed for our samples but, however, our results indicated that the shrinkage effect is the dominant phenomenon. This was evidenced by the diminution of optical gap values [inset of Fig. 2(b)] as thickness (and carrier concentration) increased. As will be discussed later, we attribute this behavior of our samples to their polycrystalline structure and to the fact that the carrier mobility is dominated by grain boundary effects.

The XRD patterns of AZO films with different thicknesses are shown in Fig. 3. All samples presented the characteristic diffraction peaks of hexagonal wurtzite ZnO (JCPDS N°36-1451). We have marked with an asterisk (*) the peak centered at $2\theta = 38.55°$, present in all patterns, which is due to a secondary $ZnAl_2O_4$ phase [28]. The presence of strong and sharp peaks indicated that the films possessed crystalline domains. The thinnest sample presented three clear diffraction peaks, (1 0 1), (0 0 2) and (1 0 3), evidencing a strong orientation in the [0 0 2] direction.

The preferential orientation of *c* axis in ZnO layers leads to an enhancement of the (0 0 2) diffraction peak [27,29]. When our films grew thicker than 0.80 μm, the (1 0 1) and (1 0 2) peaks presented slightly higher intensities, and the peak (0 0 2) remained as dominant. In turn, when the thickness increased to around 1.44 μm (~30 min), the (0 0 2) diffraction peak was still dominant while the other peaks resulted slightly diminished. Some authors suggest that for thick enough AZO films, the surface tends to be oriented in the [0 0 2] direction due to its lower surface energy [30]. The fact that such small intensities were observed for (1 0 1), (1 0 2) and (1 0 3) diffraction peaks, can be attributed to a growth competition between neighboring crystals according to their orientations. The faster growing crystals will grow over the slower ones. This competitive growth represents an orientation selection among the crystals and results in what is called the competitive growth texture [22], which explains the diminished intensity of the diffraction peaks in our samples [31].

To further investigate the difference between the films exhibiting a *c* axis or (0 0 2) preferential orientation and the intensity reduction of the other diffraction peaks, we performed mosaicity measurements by XRD. This allowed us to analyze the crystalline homogeneity of the material. The rocking curves around the diffraction angle of maximum intensity

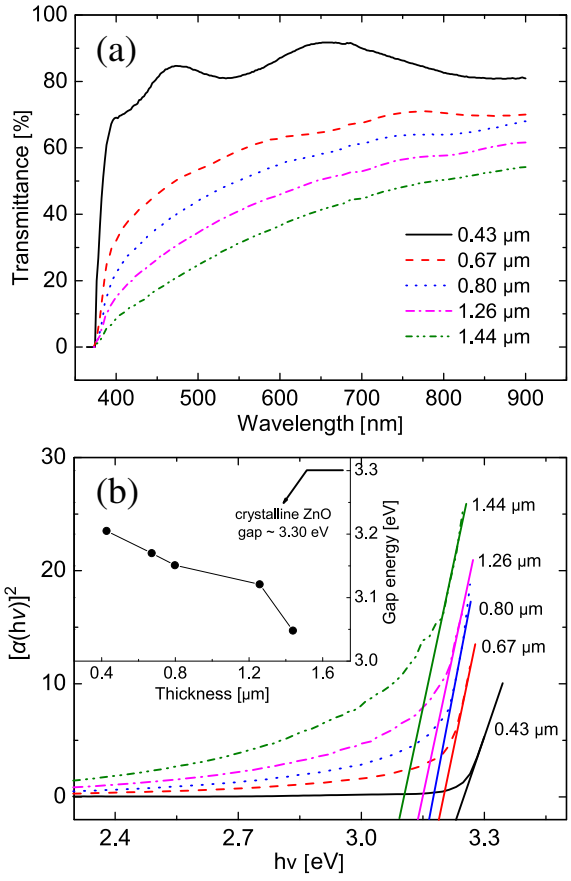

Fig. 2. (a) Optical transmittance spectra and (b) absorption coefficient curves of AZO films with different thickness. The inset of (b) presents the determined optical gap values.

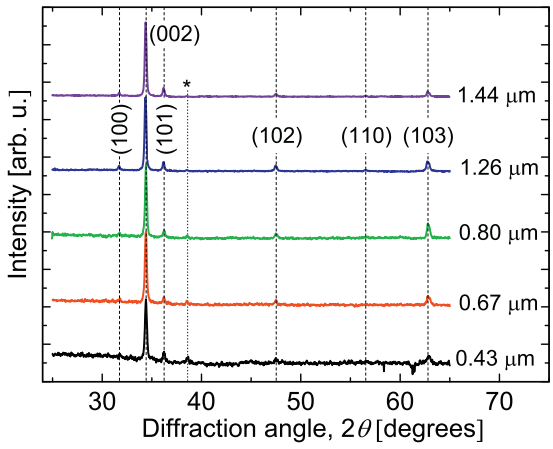

Fig. 3. X-ray diffraction patterns of AZO layers with different thicknesses, showing the characteristic ZnO crystalline peaks.

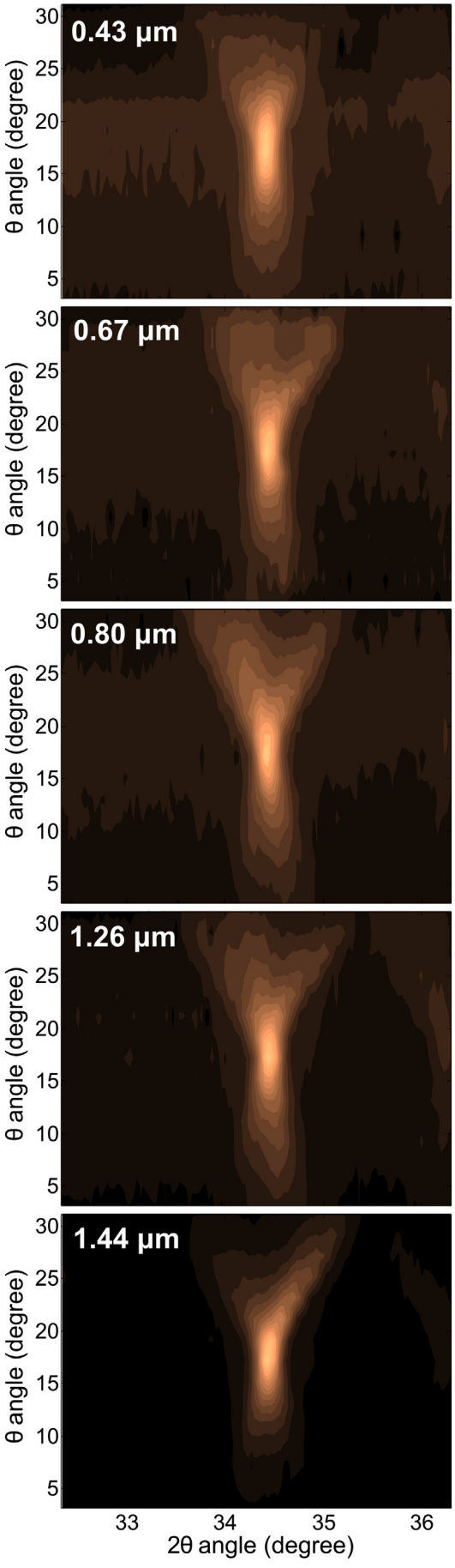

Fig. 4. Contour maps (θ, 2θ) of the films with different thicknesses, determined by XRD measurements. The graphs are centered at the ZnO (0 0 2) peak position, $2\theta = 34.3°$ and $\theta = 2\theta/2 = 17.15°$.

were obtained as described before and explained in more detail in a previous work [12]. In Fig. 4 we present the contour maps obtained for each film.

These maps correspond to the ZnO characteristic (0 0 2) diffraction peak, since it is present in all samples (see Fig. 3). They were acquired by varying the incidence angle between 3.15° and 31.15° in 2° steps and scanning the diffracted intensity along 2θ, as usual, between 32.3° and 36.3°. For the 0.43 μm-thick sample, an intense (0 0 2) peak was seen at $2\theta = 34.3°$, which was better defined and more intense for a thickness of 1.44 μm. In turn, for the 0.67, 0.80 and 1.26 μm samples the peak was slightly broader along 2θ than for the 0.43 and 1.44 μm samples. We also observed that the intensity of the (0 0 2) peak decreased along the θ axis out of the center (located at $\theta = 17.15°$ and $2\theta = 34.3°$). For 0.43 μm-thick sample, the peak was symmetric with respect to the center, which indicated that many (0 0 2) planes in the film were parallel to the substrate. This symmetry was lost as the thickness increased. For thicknesses between 0.67 and 1.44 μm, the contour maps looked slightly asymmetric along the θ axis, which indicated that the (0 0 2) planes were inclined with respect to the substrate surface.

The contour maps showed that the intensity distribution of the (0 0 2) peak for thicknesses above 0.67 μm was much broader than for 0.43 μm. This can be better understood by observing the rocking curves. Normally, the decrease of the full width at half maximum (FWHM) value obtained from the integrated intensity distribution as a function of $\Delta\theta$ is mainly due to the increase of grain size and the reduction of strain in the films. Hence, the crystal quality can be improved by increasing film thickness.

Fig. 5 illustrates the FWHM evolution of the rocking curves for the (0 0 2) peak as the thickness of AZO films increased. A typical rocking curve is showed in the inset of Fig. 5, for the 0.43 μm sample. The FWHM increased from 12.8° for a thickness of 0.43 μm to 18° for 0.80 μm. For the highest thickness (1.44 μm) the FWHM decreased to 15°. These FWHM values of the (0 0 2) rocking curves revealed the average uniformity of the *c* axis orientation throughout the volume of the films. A smaller FWHM means better uniformity in the orientation of the *c* axis and, consequently, better crystalline quality. The dependence of FWHM with thickness is also due to stress in the films. In an epitaxial growth it is generally expected that thicker films exhibit smaller FWHM values in their rocking curves and a higher crystalline quality. This can be explained as follows. At the initial stages of deposition there is an important structural mismatch between the ZnO film and the substrate, which results in large strain within the growing film, which disturbs the uniformity of the *c* axis orientation. As the film grows the strain between newer and older layers is relaxed, yielding a more ordered structure and a rocking curve with a reduced FWHM [17,32,33].

The FWHM values of our samples presented a different behavior as a function of thickness, which we attributed to the fact that film may not grow epitaxially onto the glass substrates. During initial growth stages, as said before, various grain orientations compete [34]. Also, the average grain size increases as the fastest growing grains dominate over differently oriented neighboring grains. In this case, the nucleation density is greater than the grain density. In our case, consequently, a maximum value of the FWHM was observed for the 0.80 μm-thick sample. This is attributed to the presence of internal strain in the films. For thicker samples the strain is relaxed, as mentioned above, leading to a subsequent FWHM diminution. Therefore, the FWHM curve of Fig. 5 clearly shows a transition point from high to low stress in the films for a thickness of 0.80 μm.

The variation of the conductivity of the films as a function of thickness is shown in Fig. 6. It increased from 0.3 to 50 Ω^{-1} cm^{-1} for

thicknesses ranging from 0.43 to 1.26 μm, respectively. For the 1.44 μm-thick sample the conductivity slightly decreased.

In Fig. 7 we show the variation of carrier concentration and Hall mobility as a function of thickness. We could see a linear increase of carrier concentration as samples thickened, which was of about three orders of magnitude. On the other hand, there was a decrease of carrier mobility.

The conductivity, σ, is proportional to the product between carrier concentration, n, and mobility, μ. In this way, the variation of conductivity with thickness is linked to the variations of n and μ, which are characteristic parameters that reflect the film structure and the impurity concentration. In our samples, the dopant concentration was kept constant in the precursor solution. Normally, this concentration yields different doping levels in the deposited films. Furthermore, the carriers may in part be excited from native defects such as interstitial Zn atoms and/or oxygen vacancies [35].

Therefore, the carrier concentration shown in Fig. 7 accounts for all free electrons excited from Al atoms and native defects. In consequence, we conclude that Al atoms and native defects, both acting as donors, increase free carrier concentration as the films thicken. On the other hand, the ZnO films showed low conductivity due to the chemisorption of oxygen [36,37] at grain boundaries (we recall that air was used as gas carrier during deposition). When the deposition is performed at low temperatures (~150 °C) [36], oxygen is chemisorbed in the film both at grain boundaries and at the surface. The rapid cooling at the end of deposition does not allow oxygen to escape from the sample. However, considering the higher temperature used in this work (450 °C), oxygen would have more available thermal energy to escape and increase the final carrier concentration of the samples. So, adsorbed oxygen may produce potential barriers which hinder the electrical transport. The principal chemisorption species in ZnO are O_2^{-1} at low temperatures. When deposition temperature raises, the chemisorbed O_2^{-1} desorbs from the sample and donates an electron to ZnO (i.e. $O_2^{-1} \rightarrow O_2 + e^-$) [37]. This reaction produces an increase of film conductivity. Besides this, we can consider that the surface area of the sample increases as it thickens, which also increases the fraction of free electrons trapped by chemisorbed oxygen and subsequently donated during oxygen desorption. This fact was evidenced by the results showed in Fig. 2(b), where the shift in the absorption edge was attributed to a higher carrier concentration [20,21]. It is important to note here the strong correlation observed between measured carrier concentration and obtained optical gap values.

As is also observed in Fig. 7, Hall mobility decreased for thicker samples. Carrier mobility is related to macroscopic and microscopic imperfections in the films. At the macroscopic level we include grain boundaries, internal stress and surface roughness, all of which can be observed in XRD and AFM measurements. In turn, the microscopic level accounts for ionized donors and neutral impurity atoms. In ZnO, particularly, a surface barrier is created by the chemisorption of oxygen, which considerably reduces carrier mobility. Besides this, grain boundaries are also considered to be effective inhibitors of carrier mobility [36].

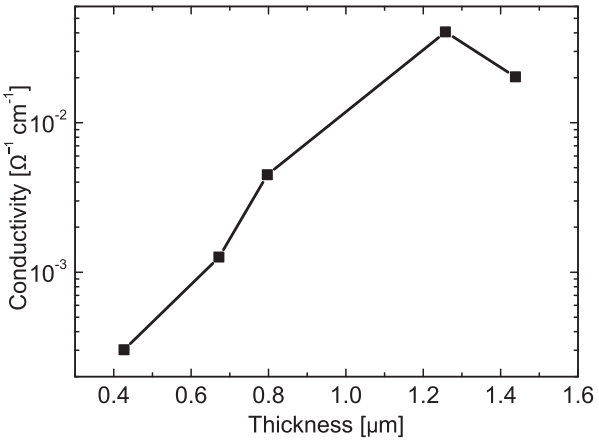

Fig. 6. Conductivity of the films as a function of thickness. Dotted lines are only a guide to the eye.

Carrier mobility in thinner AZO films, with lower RMS roughness, resulted strongly dependent on thickness. However, it remained constant for thicknesses between 0.80 and 1.26 μm. We consider that the thickness dependence of mobility in AZO films is mainly due to a variation in the density of scattering centers, such as lattice strain points, and dislocations caused by misorientation between crystalline domains (mosaicity). The mobility of the thickest film (1.44 μm) reached a minimum value, although the FWHM value of its rocking curve was slightly lower than for the 1.26 μm sample. This might be indicating that the defect density increased for higher deposition times and that other scattering centers (such as grain boundaries) were introduced in the film. Thus, we conclude that the density of scattering centers increases with deposition time resulting in reduced carrier mobility.

The electrical conductivity can be modeled as an activated process, following the Arrhenius law in a wide temperature range. This can be expressed as

$$\sigma(T) = \sigma_0 \exp\left(-\frac{E_a}{k_B T}\right), \quad (1)$$

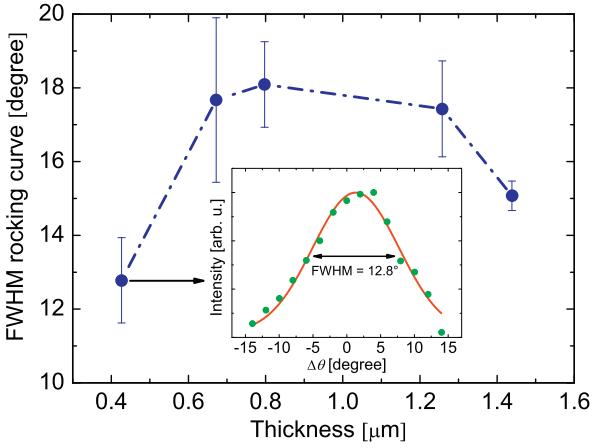

Fig. 5. Full-width at half maximum values of the rocking curves as a function of film thickness, determined for the (0 0 2) diffraction peak. The inset shows the fitting procedure (for the 5 min sample) to determine the FWHM value.

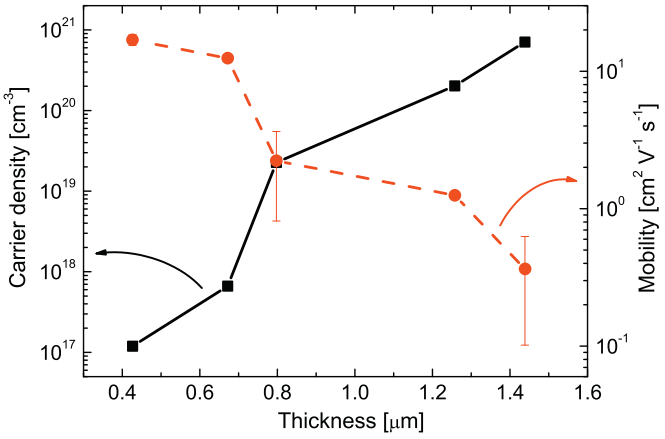

Fig. 7. Carrier concentration and Hall mobility as a function of thickness. Dotted lines are only a guide to the eye.

where E_a is the characteristic activation energy of the process, T is the absolute temperature, k_B is Boltzmann constant and σ_0 is a nearly constant prefactor [38]. In ZnO, the activation energy is related to localized states in the semiconductor gap and is generally taken as the energy difference between the minimum (maximum) of the conduction (valence) band and the Fermi energy, if the semiconductor is *n*-type (*p*-type).

Fig. 8(a) presents the curves of current as a function of temperature determined for each sample. These curves presented an activated transport mechanism, in accordance with Eq. (1), with low activation energies. This evidenced that the samples were highly doped and that their Fermi levels laid just below the conduction band. In turn, Fig. 8(b) shows the activation energies calculated by fitting of the Arrhenius plots of current as a function of temperature. The obtained values were all in the range between 20 and 60 meV, which is in good agreement with other works [39]. As mentioned before, we attribute these very low activation energies to grain boundary effects dominating carrier mobility. The presence of grain boundaries was evidenced by the existence of a high degree of mosaicity between crystalline domains in the samples. The defective structure of grain boundaries is known to contribute with localized defect states in the material band gap which may act as traps or recombination centers. In thicker films, with a higher degree of mosaicity, these effects become more important and are mainly mediated by oxygen ions chemisorbed in ZnO boundaries, as discussed above. Therefore, when these species are desorbed they donate an electron to ZnO (see reaction above [37]). As these electrons are trapped they set up a negative charge at the grain boundaries, generating a spatial charge region extending into the grains and giving place to the observed low activation energies. This is consistent with the observed diminution of the activation energy for thicker samples, which is due to the presence of a higher amount of intrinsic defects in the films, and is also consistent with the lower mobility of the thickest sample (1.40 μm), because of higher carrier density.

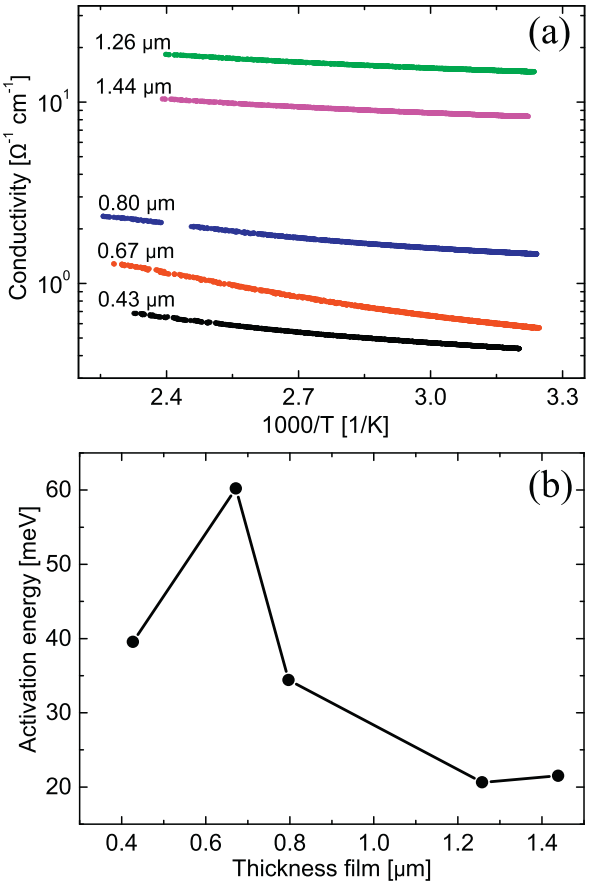

Fig. 8. Results obtained from (a) dark current measurements and (b) activation energy calculations as a function of thickness. Dotted lines are only a guide to the eye.

Besides the fact that grain boundaries dominate because of their much higher density of defects, there is also a small contribution from defects inside crystalline domains, like Zn interstitials (Zn_i) and oxygen vacancies (V_O). Also the group-III impurities like Al act as shallow donors in ZnO when substituting Zn atoms. The extra valence electron of these impurities is loosely bound and occupies effective-mass states near the conduction band minimum at low temperatures. As the temperature rises, this extra electron is easily excited to the conduction band.

4. Conclusion

We have obtained Al-doped ZnO thin films on glass with different thicknesses through sol–gel synthesis and spray pyrolysis deposition at 450 °C. We analyzed the correlation between morphological characteristics, like RMS roughness, grain size, preferential growth orientation and mosaicity, with electrical characteristics, like conductivity, mobility and carrier concentration, and their evolution with film thickness. In all samples, we obtained high conductivities, in the order of 50 Ω^{-1} cm^{-1}, and moderate Hall mobilities, of about 5 cm^2 V^{-1} s^{-1}. We found that by increasing film thickness the mosaicity between crystalline domains results greater. This has a direct influence on conductivity and carrier concentration, since thicker films yielded higher conductivities and higher carrier concentrations. Also, the optical gap energy showed a blue shift. Therefore, the results presented demonstrate the strong influence the spray pyrolysis growth parameters have on the electrical properties of the ZnO thin films. In particular the thickening effect has a marked effect on carrier concentration and activation energies for electrical conduction, attributed mainly to the defective structure of grain boundaries.

Acknowledgments

This work was partially supported by projects from ANPCyT (PICT 32515), Universidad Nacional del Litoral (CAID 2009/68-343) and CONICET (PID 1464). We also acknowledge the technical support of Ramón Saavedra.

References

[1] X.T. Hao, F.R. Zhu, K.S. Ong, L.W. Tan, Semicond. Sci. Technol. 21 (2006) 48.
[2] C.G. Granqvist, Sol. Energy Mater. Sol. Cells 91 (2007) 1529.
[3] T. Minami, Thin Solid Films 516 (2008) 5822.
[4] Y. Natsume, H. Sakata, Thin Solid Films 372 (2000) 30.
[5] B.J. Lokhande, M.D. Uplane, Appl. Surf. Sci. 167 (2000) 243.
[6] C.R. Gorla, N.W. Emanetoglu, S. Liang, W.E. Mayo, Y. Lu, M. Wraback, H. Shen, J. Appl. Phys. 85 (1999) 2595.
[7] J.H. Choi, H. Tabata, T. Kawai, J. Cryst. Growth 226 (2001) 493.
[8] D.M. Bagnall, Y.F. Chen, Z. Zhu, T. Yao, S. Koyama, M.Y. Shen, T. Goto, Appl. Phys. Lett. 70 (1997) 2230.
[9] K. Ellmer, J. Phys. D. Appl. Phys. 33 (2000) R17.
[10] D.F. Paraguay, J. Morales, L.W. Estrada, E. Andrade, M. Miki-Yoshida, Thin Solid Films 366 (2000) 16.
[11] T. Prasada Rao, M.C. Santhosh Kumar, N. Sooraj Hussain, J. Alloys Compd. 541 (2012) 495.
[12] F.A. Garcés, N. Budini, R.R. Koropecki, R.D. Arce, Thin Solid Films 531 (2013) 172.
[13] L. Znaidi, Mater. Sci. Eng. B 174 (2010) 18.
[14] R.R. Biswal, S. Velumani, B.J. Babu, A. Maldonado, S. Tirado-Guerra, L. Castañeda, M. de la L. Olvera, Mater. Sci. Eng. B 174 (2010) 46.
[15] B. Marty, P. Moretto, P. Gergaud, J.L. Lebrun, K. Ostolaza, V. Ji, Acta Mater. 45 (1997) 791.
[16] M. Mekhnache, A. Drici, L. Saad Hamideche, H. Benzarouk, A. Amara, L. Cattin, J.C. Bernède, M. Guerioune, Superlattice. Microst. 49 (2011) 510.
[17] J.I. Owen, W. Zhang, D. Köhl, J. Hüpkes, J. Cryst. Growth 344 (2012) 12.
[18] S.M. Lan, W.Y. Uen, C.E. Chan, K.J. Chang, S.C. Hung, Z.Y. Li, T.N. Yang, C.C. Chiang, P.J. Huang, M.D. Yang, G.C. Chi, C.Y. Chang, J. Mater. Sci: Mater. Electron. 20 (2009) 441.
[19] G. Harbeke, L. Jastrzebski, J. Electrochem. Soc. 137 (1990) 696.
[20] A.P. Roth, J.B. Webb, D.F. Williams, Phys. Rev. B 25 (1982) 7836.
[21] B.E. Sernelius, K.F. Berggren, Z.C. Jin, I. Hamberg, C. Granqvist, Phys. Rev. B 37 (1988) 10244.
[22] S.S. Lin, J.L. Huang, Surf. Coat. Technol. 185 (2004) 222.

[23] A.N. Banerjee, C.K. Ghosh, K.K. Chattopadhyay, H. Minoura, A.K. Sarkar, A. Akiba, A. Kamiya, T. Endo, Thin Solid Films 496 (2006) 112.
[24] H.P. He, F. Zhuge, Z.Z. Ye, L.P. Zhu, F.Z. Wang, B.H. Zhao, J. Appl. Phys. 99 (2006) 023503.
[25] M. Suchea, S. Christoulakis, N. Katsarakis, T. Kitsopoulos, G. Kiriakidis, Thin Solid Films 515 (2007) 6562.
[26] M. Bouderbala, S. Hamzaoui, M. Adnane, T. Sahraoui, M. Zerdali, Thin Solid Films 517 (2009) 1572.
[27] M.A.L. Lopez, A. Maldonado, R.C. Perez, G.T. Delgado, M. de la L. Olvera, Sol Energy Mater Sol Cells 90 (2006) 2362.
[28] T. Wei, Y. Zhang, Y. Yang, R. Tan, P. Cui, W. Song, Surf. Coat. Technol. 221 (2013) 201.
[29] M.H. Huang, S. Mao, H. Feick, H. Yan, Y. Wu, H. Kind, E. Weber, R. Russo, P. Yang, Science 292 (2001) 1897.
[30] N. Fujimura, T. Nishihara, S. Goto, J. Xu, T. Ito, J. Cryst. Growth 130 (1993) 269.
[31] P.M.R. Kumar, C.S. Kartha, K.P. Vijayakumar, T. Abe, Y. Kashiwaba, F. Singh, D.K. Avasthi, Semicond. Sci. Technol. 20 (2005) 120.
[32] J. Perrière, E. Millon, W. Seiler, C. Boulmer-Leborgne, V. Craciun, O. Albert, J.C. Loulergue, J. Etchepare, J. Appl. Phys. 91 (2002) 690.
[33] B.Z. Dong, G.J. Fang, J.F. Wang, W.J. Guan, X.Z. Zhao, J. Appl. Phys. 101 (2007) 033713.
[34] A. van der Drift, Philips Res. Rep. 22 (1967) 267.
[35] Y. Igasaki, H. Saito, J. Appl. Phys. 69 (1991) 2190.
[36] Y. Igasaki, H. Saito, J. Appl. Phys. 70 (1991) 3613.
[37] T. Prasada Rao, M.C. Santhoshkumar, Appl. Surf. Sci. 255 (2009) 4579.
[38] V. Aquilanti, K.C. Mundim, S. Cavalli, D. De Fazio, A. Aguilar, J.M. Lucas, Chem. Phys. 398 (2012) 186.
[39] A. Janotti, C.G. Van de Walle, Rep. Prog. Phys. 72 (2009) 126501.